

Crystallization transformations in vacuum-deposited amorphous aluminum fluoride self-developing thin-film resists induced by electron-beam irradiation

G. S. Chen^{a)}

Department of Materials Science, Feng Chia University, Taichung 407, Taiwan

P. Y. Lee

Institute of Materials Engineering, Taiwan Ocean University, Keelung 202, Taiwan

C. B. Boothroyd and C. J. Humphreys

Department of Materials Science and Metallurgy, University of Cambridge, Cambridge CB2 3QZ, United Kingdom

(Received 14 August 2001; accepted 4 February 2002)

Conventional transmission electron microscopy is employed to investigate *in situ* electron-beam-induced phase transformations in vacuum-deposited amorphous aluminum fluoride (*a*-AlF₃) self-developing thin-film resists. The *a*-AlF₃ resists exhibit a very complex sequence of crystallization transitions with three crystalline materials (Al, AlF₃, and Al₂O₃) formed sequentially as the electron dose increases from 10⁵ to 10⁷ Cm⁻². Thermally evaporated “dry” *a*-AlF₃ is dissociated into Al crystalline colloids at a threshold dose of $\sim 1 \times 10^5$ Cm⁻², and begins to transform into crystalline AlF₃ (*c*-AlF₃) at a dose of $\sim 1 \times 10^6$ Cm⁻². However, water contained in the “wet” films accelerates the transition of *a*-AlF₃ to *c*-AlF₃ at a reduced threshold dose of $\sim 2 \times 10^5$ Cm⁻². Moreover, *a*-AlF₃ films prepared by electron-beam deposition require a markedly different dose for each substance to crystallize, attributed to a microstructure variation. For all of the *a*-AlF₃ films, textured Al₂O₃ is formed at doses of $\geq 1 \times 10^7$ Cm⁻², also with the aid of H₂O absorbed from the microscope vacuum and by the following chemical reaction: $2\text{AlF}_{3(s)} + 3\text{H}_2\text{O}_{(g)} \rightarrow \text{Al}_2\text{O}_{3(s)} + 6\text{HF}_{(g)}$. © 2002 American Vacuum Society. [DOI: 10.1116/1.1464842]

I. INTRODUCTION

Vacuum-deposited amorphous AlF₃ (*a*-AlF₃) thin films have been used by several research groups to fabricate nanostructures.^{1–5} Under the impingement of a finely focused electron beam of current densities typically 10⁵–10⁷ A m⁻², the exposed site can be self-developed, subsequently forming a variety of nanometer-sized features (such as holes and trenches) of sizes less than 5 nm. Previous investigations usually assumed that the self-developing behavior of *a*-AlF₃ thin-film resists was unaffected by the films’ humidity or environmental factors. However, evaporated *a*-AlF₃ thin films are normally porous and thus easily absorb varying amounts of water, some of which is chemically bonded to AlF₃ and some of which is physisorbed on the surface and in the pores.^{6,7} We have previously demonstrated that thermally evaporated *a*-AlF₃ thin films undergo a sequence of phase-transition processes, which are highly sensitive to the presence of water, if damaged using a broad beam of electrons in a transmission electron microscope (TEM).⁸ In this article the electron-beam-induced phase-transition behavior of thermally evaporated and electron-beam (*e*-beam) deposited *a*-AlF₃ thin-film resists is further investigated. Factors influencing the transformation of the new crystalline phases (Al, AlF₃, and Al₂O₃) and the self-developing behavior of vacuum-deposited AlF₃ resists are also discussed.

^{a)}Electronic mail: gschen@fcu.edu.tw

II. EXPERIMENTAL PROCEDURES

All of the *a*-AlF₃ thin films were deposited by an Edwards Auto 306 vacuum coater. Three types of sample films were examined: thermally evaporated “dry” films, thermally evaporated “wet” films, and *e*-beam deposited “dry” films, all three being coated directly on self-supporting amorphous carbon films (5 nm thick) on 3 mm copper grids. The thicknesses of the films, as measured with a quartz crystal monitor, were all ~ 50 nm ($\pm 2\%$). For the thermally evaporated and *e*-beam deposited dry films, anhydrous AlF₃ powder was dehydrated at 400 °C for 10 h to remove the absorbed water completely prior to evaporation. For the wet films, AlF₃ · 3H₂O powder was evaporated thermally without preheating. The two (thermal and *e*-beam) dry films were deposited at a lower pressure of around 5×10^{-4} Pa ($\sim 4 \times 10^{-6}$ Torr), whereas the wet *a*-AlF₃ films were thermally evaporated at a markedly higher pressure of $\sim 10^{-2}$ Pa. Such an enormous increase in the background pressure is due to the release of H₂O from the hydrated AlF₃ · 3H₂O. The amount of H₂O absorbed to the AlF₃ films was examined using Fourier transform infrared spectroscopy (FTIR) to identify the O–H absorption band at $0.33 \mu\text{m}^{-1}$.

All films were freshly prepared and transferred to a JEOL 2000FX transmission electron microscope within 15 min of preparation. Beam-irradiation experiments were carried out *in situ* with the microscope operating at an acceleration voltage of 100 kV in conjunction with a Gatan parallel electron loss spectrometer (EELS). The beam current was

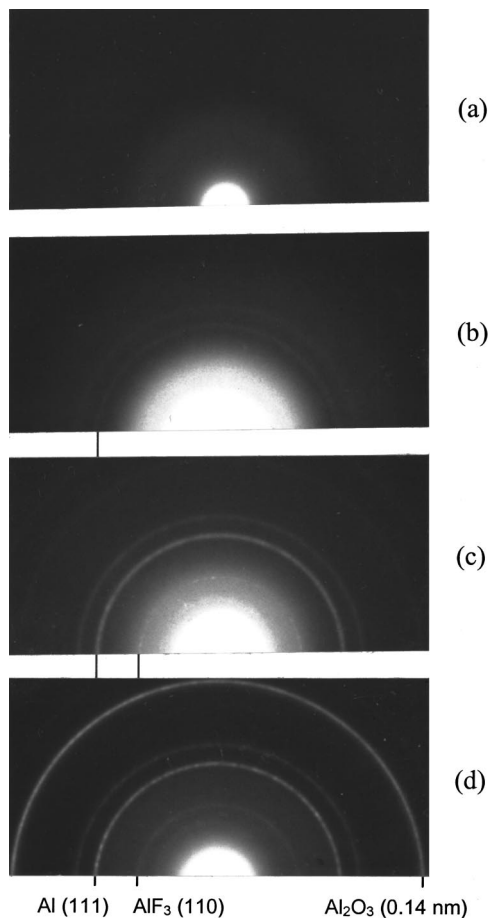


FIG. 1. Set of electron diffraction patterns illustrating that (a) thermally evaporated dry *a*-AlF₃ films undergo a sequence of complex phase transitions, forming (b) Al ($1.3 \times 10^5 \text{ Cm}^{-2}$), (c) *c*-AlF₃ ($\sim 1 \times 10^6 \text{ Cm}^{-2}$), and (d) textured Al₂O₃ ($1 \times 10^7 \text{ Cm}^{-2}$).

measured using a Faraday cage at the side of the specimen, which was set at 31.1 nA and routinely checked every 10 min, making sure that any decay of the beam current was compensated for. The condenser lens C2 was overfocused to give a uniform irradiation area of $4.5 \times 10^{-12} \text{ m}^2$ (or $8.0 \times 10^{-12} \text{ m}^2$). This adjustment led to damage of the films by a probe of current density $6.9 \times 10^3 \text{ A m}^{-2}$ (or $3.9 \times 10^3 \text{ A m}^{-2}$). The same area of the specimen was irradiated throughout each experiment, with the irradiation being stopped at frequent intervals for a series of selected area diffraction patterns to be obtained. These selected area diffraction patterns were all obtained under identical exposure and plate-developing conditions, thereby facilitating direct comparisons of all the patterns by measuring the intensities of diffraction rings.

III. RESULTS AND DISCUSSION

Four diffraction patterns from a prolonged damage series of a thermally evaporated dry film are shown in Figs. 1(a)–1(d). It can be seen from this set of figures that the as-deposited amorphous AlF₃ film originally contains only diffuse rings [Fig. 1(a)], and begins yielding sharp diffraction rings of Al and crystalline AlF₃ (*c*-AlF₃) at doses of ~ 1

$\times 10^5$ and $\sim 1 \times 10^6 \text{ Cm}^{-2}$, respectively [Figs. 1(b) and 1(c)]. After prolonged irradiation with a dose of $1 \times 10^7 \text{ Cm}^{-2}$, a strong 0.14-nm Al₂O₃ diffraction ring emerges [Fig. 1(d)]. It is interesting to note that tilting the specimen did not reveal any visible change in the intensities of Al and AlF₃ rings. However, when adequately tilted, the 0.14-nm Al₂O₃ diffraction ring changed to two arcs, along with the appearance of four arcs centered at 0.197 nm. This finding indicates that the Al₂O₃ crystals possess a textured structure.⁹

Dark field images, carefully recorded from *a*-AlF₃ films by placing an objective aperture on diffuse rings of Fig. 1(a), exhibit a speckle contrast also reminiscent of an amorphous structure [see Fig. 2(a)]. As evidenced from the Al (111) dark field image in Fig. 2(b), an electron dose of $\sim 1 \times 10^5$ (or 2×10^5) Cm^{-2} has already produced many Al equiaxed crystallites of sizes ≤ 10 nm. Gradually increasing the dosage caused the Al crystallites to grow equilaterally. Ultimately at doses of $\geq 1 \times 10^6 \text{ Cm}^{-2}$, crystalline Al colloids of sizes from 5 to 30 nm were observed. Dark field images recorded from AlF₃ (110) reveal that a dose of $\geq 1 \times 10^6 \text{ Cm}^{-2}$ is required to produce a significant amount of AlF₃ nanocrystallites [see Fig. 2(c)]. Al₂O₃ textured crystallites, which distribute evenly throughout the matrix, can be observed only at a substantially high electron dose of $1 \times 10^7 \text{ Cm}^{-2}$ or greater. [Fig. 2(d)]. Recording a highly magnified dark field image such as that depicted in Fig. 2 requires a dose of at least $5 \times 10^4 \text{ Cm}^{-2}$. Therefore characterizing the phase-transition behavior of the *a*-AlF₃ films simply by using TEM imaging is difficult because the dosage needed to record a micrograph inevitably damages the films seriously. Conversely, the dosage received by a film during the recording of a selected area electron diffraction pattern can be optimized to only $3 \times 10^2 \text{ Cm}^{-2}$. Thus electron diffraction analysis was hereinafter conducted to further elucidate the phase-transition process.

The diffraction technique was performed by irradiating the same area of each film, during which the irradiation was stopped at frequent intervals for a series of selected area diffraction patterns to be recorded (for details see Sec. II). Each set of patterns was individually digitized and radially averaged to produce intensity as a function of scattering angle (2θ). Figure 3 shows the resultant diffraction intensities at four dosages for thermally evaporated dry AlF₃ films damaged at a current density of $6.9 \times 10^3 \text{ A m}^{-2}$, illustrating that the damage process proceeds with the broad peaks of *a*-AlF₃ disappearing and sharp peaks of the crystalline substances (Al, AlF₃, and Al₂O₃) appearing. (It is to be noted that the results presented herein are also typical of current density at $3.9 \times 10^3 \text{ A m}^{-2}$.) Because each plate was recorded and developed under identical conditions, the beam-induced phase-transition behavior can be assessed by directly comparing the intensities of the diffraction rings. For each of the three specimens (the thermally evaporated dry and wet films and *e*-beam deposited dry film), diffraction patterns were obtained as in Fig. 1 over a range of doses from 10^5 to 10^8 Cm^{-2} , radially averaged as in Fig. 3 and the areas under

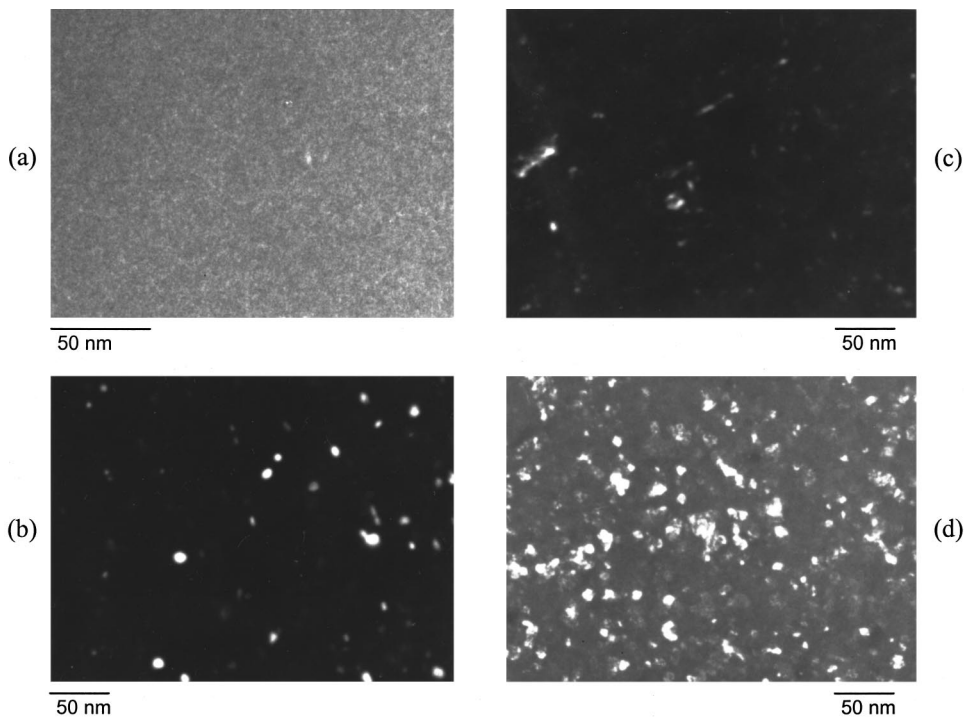


FIG. 2. Set of dark field images showing that (a) $a\text{-AlF}_3$ undergoes a sequence of phase transitions, forming (b) Al colloids ($2 \times 10^5 \text{ Cm}^{-2}$), (c) $c\text{-AlF}_3$ ($2 \times 10^6 \text{ Cm}^{-2}$), and (d) textured Al_2O_3 ($5 \times 10^7 \text{ Cm}^{-2}$).

the most prominent peak for each crystalline product found. These diffraction peak areas are plotted as a function of dosage in Figs. 4(a)–4(c), allowing the phase transformations to be compared quantitatively.

Comparing Figs. 4(a) and 4(b) reveals that, for the dry and wet thermally evaporated films, the progress of alumi-

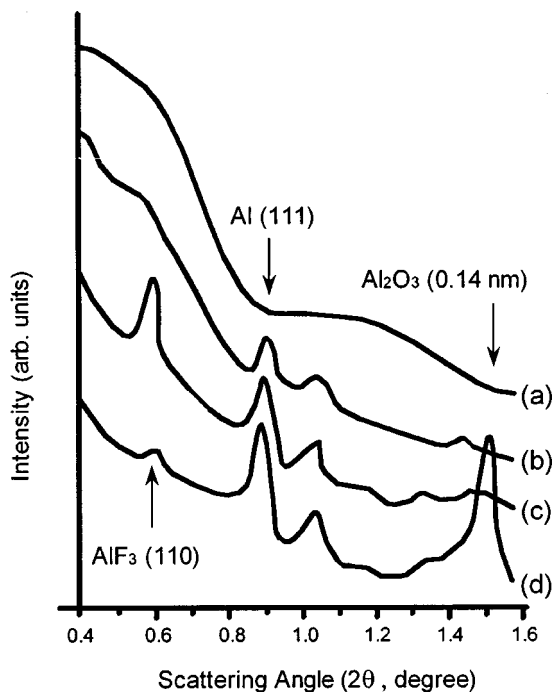


FIG. 3. Radial average of the diffraction patterns as a function of scattering angle, showing (a) $a\text{-AlF}_3$ is gradually transformed into (b) crystalline Al ($4 \times 10^5 \text{ Cm}^{-2}$), (c) $c\text{-AlF}_3$ ($2 \times 10^6 \text{ Cm}^{-2}$), and (d) Al_2O_3 ($5 \times 10^7 \text{ Cm}^{-2}$). The peak evolving just to the right of Al(111) is Al (200).

num crystallization is similar, with aluminum forming at a slightly lower dose ($\sim 1 \times 10^5 \text{ Cm}^{-2}$) in the dry film and the maximum intensity being higher by $\sim 50\%$. The amount of Al for both films levels off above a dose of $1 \times 10^6 \text{ Cm}^{-2}$. However, a much lower dose ($\sim 2 \times 10^5 \text{ Cm}^{-2}$) is needed for the $a\text{-AlF}_3$ to crystallize in the wet film than in the dry film ($\sim 1 \times 10^6 \text{ Cm}^{-2}$). In addition, if the dry film is exposed to air for a few days then the behavior of forming $c\text{-AlF}_3$ becomes more akin to that of the wet film. Although the wet film examined here was unusual in this respect, Fourier transform infrared spectroscopy showed that this film indeed exhibited an enormous O–H absorption band, whereas the O–H absorption band was absent from the dry film.⁸ This finding indicates that water accelerates the crystallization transition of $a\text{-AlF}_3$, forming $c\text{-AlF}_3$. It is to be noted that $a\text{-AlF}_3$ resists of a limited thickness range (40–120 nm) are damaged in parallel throughout the irradiated volume of the sample film.¹⁰ Thus the amounts of aluminum and $c\text{-AlF}_3$ crystallites produced within the beam/sample interaction volume (beam-volume) are expected to scale with the thickness of the sample films. As the films examined herein all have a thickness of $50 \text{ nm} \pm 2\%$, the differences in amounts of aluminum (or $c\text{-AlF}_3$) in Fig. 4 are mainly related to differences in intrinsic properties of the samples.

As Figs. 4(a) and 4(c) show, the main difference between the thermally and e-beam evaporated dry AlF_3 films is that much less aluminum is formed in the e-beam evaporated film over the whole range of dosages, while the crystallization of $a\text{-AlF}_3$ in this film behaves in a fashion similar to that of the thermal film, but with ~ 1.8 times as much $c\text{-AlF}_3$. For the e-beam film, diffraction peaks of Al in the original patterns (TEM micrographs) were rather weak over the whole range of doses from 10^5 to 10^7 Cm^{-2} . This observation suggests

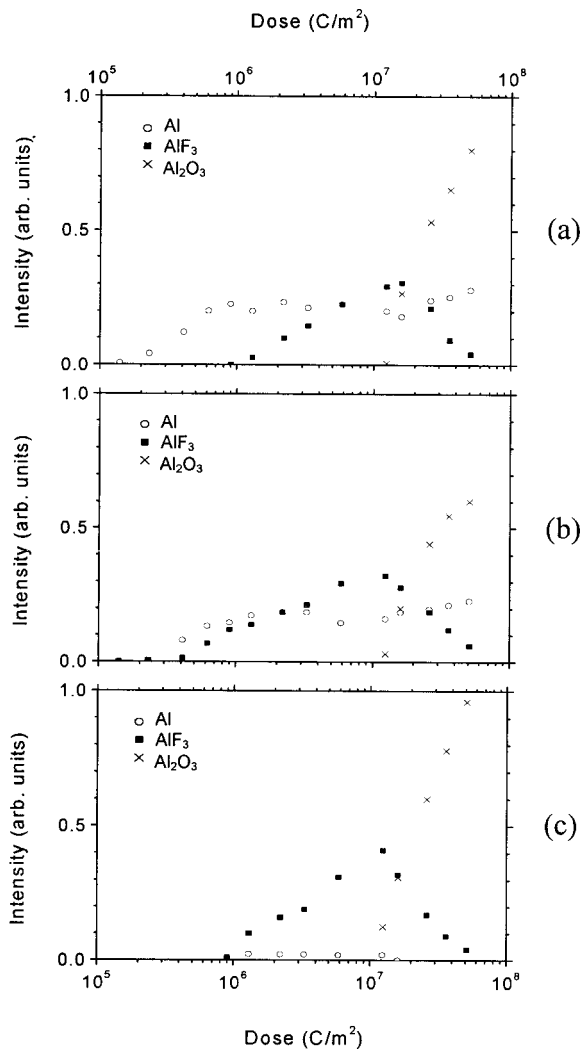


FIG. 4. Diffraction peak areas of the electron-beam-induced crystalline products of the Al (111), AlF_3 (110), and Al_2O_3 0.14-nm rings as a function of dosage for (a) dry and (b) wet thermally evaporated and (c) dry electron-beam deposited $a\text{-AlF}_3$ films.

that although the water content in the dry thermal and dry e-beam films is similar and low, there is an additional structural difference between films produced by the two deposition methods. Thermally evaporated AlF_3 films are deposited by using thermal energy alone for driving evaporation, reaction, and film structure development, while electron-beam deposited films are produced by using an energy beam (5 kW) to vaporize the AlF_3 source and to activate the surface mobility of adatoms. Thus electron-beam deposited films are normally denser than thermally evaporated films. Moreover, aluminum colloids are formed primarily by radiolytic decomposition of AlF_3 instead of beam-heating effects.¹¹ The film's microstructure (e.g., porosity) thus could be an important factor deciding the efficiency of radiolysis. As having a greater degree of porosity, the thermally evaporated films would contain a higher initial concentration of intrinsic defects, allowing radiolysis to occur easier as more interstitial/substitutional sites are available to accommodate the beam-induced defects. Indeed, *in situ* observation during damaging

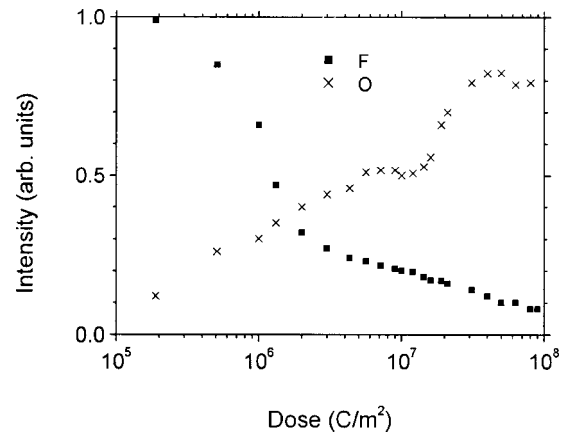


FIG. 5. Evolution of fluorine and oxygen intensities obtained from EELS spectra during electron-beam irradiation of $a\text{-AlF}_3$ films.

of the sample films with a broad beam in a TEM (or rastering by a focused probe in a dedicated scanning transmission electron microscope) revealed that irradiated volumes of thermally evaporated films lose their integrity within a short period of ~ 3 s or less, whereas those of e-beam deposited AlF_3 films can maintain their morphology for tens of seconds.

For a dry thermal $a\text{-AlF}_3$ film, measurements were made of the areas under the oxygen and fluorine K edges of EELS spectra as a function of dosage (Fig. 5). During these EELS measurements, the beam current was kept constant and the same area irradiated. It can be seen from Fig. 5 that, up to a dose of $1 \times 10^6 \text{ Cm}^{-2}$, fluorine decreases rapidly, then more slowly and at a uniform rate above this dose. $1 \times 10^6 \text{ Cm}^{-2}$ corresponds to the dose when $a\text{-AlF}_3$ starts to crystallize. Thus up to $1 \times 10^6 \text{ Cm}^{-2}$, fluorine is being lost and the AlF_3 remains amorphous. AlF_3 begins to crystallize at $1 \times 10^6 \text{ Cm}^{-2}$ and is more stable to damage. Therefore the rate of loss of fluorine decreases, corresponding to the flat of Al intensities at this dose (see Fig. 4). Our previous study¹⁰ found that the doses required for AlF_3 resists to develop fully are on the order of 10^5 Cm^{-2} . This order of doses is also required for $a\text{-AlF}_3$ to transform into Al and $c\text{-AlF}_3$. As $c\text{-AlF}_3$ is less sensitive to radiolysis than $a\text{-AlF}_3$, the efficiency of developing $a\text{-AlF}_3$ resists will be retarded by the amorphous-to-crystalline transformation of AlF_3 found in this work.

The formation of the textured Al_2O_3 in all three films at the high-dose regime ($\geq 1 \times 10^7 \text{ Cm}^{-2}$) is interesting. According to Fig. 5, the oxygen 535-eV edge is present in lightly damaged films ($\sim 2 \times 10^5 \text{ Cm}^{-2}$), but no crystalline Al_2O_3 is seen in Fig. 4. The oxygen, presumably in the form of H_2O picked up from the microscope vacuum, is gradually incorporated into the AlF_3 film as the fluorine is lost. Above $1 \times 10^7 \text{ Cm}^{-2}$, textured Al_2O_3 begins to form suddenly, corresponding to a sharp decrease in the amount of $c\text{-AlF}_3$ and an abrupt increase in the oxygen concentration at this dose (compare Figs. 4 and 5). This finding suggests that the textured Al_2O_3 is formed by a reaction between AlF_3 and H_2O . Thus the following chemical reaction equation is proposed:

$2\text{AlF}_{3(s)} + 3\text{H}_2\text{O}_{(g)} \rightarrow \text{Al}_2\text{O}_{3(s)} + 6\text{HF}_{(g)}$. As the dose exceeds $5 \times 10^7 \text{ Cm}^{-2}$, the concentration of oxygen levels off when all the AlF_3 has reacted, and Al_2O_3 may itself be decomposing due to irradiation.¹²

IV. CONCLUSION

We have shown that the electron-beam damage of self-developing *a*- AlF_3 thin-film resists is a very complex process whereby crystalline aluminum is formed first at doses of $\geq 1 \times 10^5 \text{ Cm}^{-2}$ as fluorine is lost, followed by the crystallization of the *a*- AlF_3 into *c*- AlF_3 normally at $1 \times 10^6 \text{ Cm}^{-2}$. At doses of $\geq 1 \times 10^7 \text{ Cm}^{-2}$, the oxygen (presumably due to water) in the microscope ambient reacts with the AlF_3 to form textured Al_2O_3 . It is important to note that both the water content of the films and the deposition method can greatly alter the dosage required for each crystalline substance to form. The alternation of the phase transitions by these factors has implications for nanofabrication of self-developing inorganic electron-beam resists.

ACKNOWLEDGMENTS

The authors would like to thank the National Science Council of the Republic of China for financially supporting the publication of this research under Contract No. NSC 87-2613-M-035-001.

- ¹A. Muray, M. Isaacson, and I. Adesida, *Appl. Phys. Lett.* **45**, 589 (1984).
- ²J. C. Hollenbeck and R. C. Buchanan, *J. Mater. Res.* **5**, 1058 (1990).
- ³V. I. Nikolaichik, *Philos. Mag. A* **68**, 227 (1993).
- ⁴Y. Ito, A. L. Bleloch, S. J. R. Granleese, and L. M. Brown, *Inst. Phys. Conf. Ser.* **138**, 507 (1993).
- ⁵G. S. Chen and C. J. Humphreys, *J. Vac. Sci. Technol. B* **15**, 1954 (1997).
- ⁶A. P. Bradford, G. Hass, and M. McFarland, *Appl. Opt.* **11**, 2242 (1972).
- ⁷J. D. Targove, B. G. Bovard, L. J. Lingg, and H. A. Macleod, *Thin Solid Films* **159**, L57 (1988).
- ⁸G. S. Chen, C. B. Boothroyd, and C. J. Humphreys, *Appl. Phys. Lett.* **69**, 170 (1996).
- ⁹P. B. Hirsch, A. Howie, R. B. Nicholson, D. W. Pashley, and M. J. Whelan, *Electron Microscopy of Thin Crystals* (Krieger, New York, 1977), p. 117.
- ¹⁰G. S. Chen and C. J. Humphreys, *J. Appl. Phys.* **85**, 148 (1999).
- ¹¹M. E. Mochel, J. A. Eades, M. Metzger, J. I. Meyer, and J. M. Mochel, *Appl. Phys. Lett.* **44**, 502 (1984).
- ¹²C. J. Morgan, S. J. Bailey, A. R. Preston, and C. J. Humphreys, *Inst. Phys. Conf. Ser.* **119**, 503 (1991).